J Arid Land (2024) 16(3): 331–354
https://doi.org/10.1007/s40333-024-0054-7

Science Press Springer-Verlag

Improving the accuracy of precipitation estimates in a typical inland arid area of China using a dynamic Bayesian model averaging approach

XU Wenjie[1,2], DING Jianli[1,2*], BAO Qingling[1,2], WANG Jinjie[1,2], XU Kun[1,2]

[1] College of Geography and Remote Sensing Sciences, Xinjiang University, Urumqi 830017, China;
[2] Key Laboratory of Smart City and Environment Modelling of Higher Education Institute, Xinjiang University, Urumqi 830017, China

Abstract: Xinjiang Uygur Autonomous Region is a typical inland arid area in China with a sparse and uneven distribution of meteorological stations, limited access to precipitation data, and significant water scarcity. Evaluating and integrating precipitation datasets from different sources to accurately characterize precipitation patterns has become a challenge to provide more accurate and alternative precipitation information for the region, which can even improve the performance of hydrological modelling. This study evaluated the applicability of widely used five satellite-based precipitation products (Climate Hazards Group InfraRed Precipitation with Station (CHIRPS), China Meteorological Forcing Dataset (CMFD), Climate Prediction Center morphing method (CMORPH), Precipitation Estimation from Remotely Sensed Information using Artificial Neural Networks-Climate Data Record (PERSIANN-CDR), and Tropical Rainfall Measuring Mission Multi-satellite Precipitation Analysis (TMPA)) and a reanalysis precipitation dataset (ECMWF Reanalysis v5-Land Dataset (ERA5-Land)) in Xinjiang using ground-based observational precipitation data from a limited number of meteorological stations. Based on this assessment, we proposed a framework that integrated different precipitation datasets with varying spatial resolutions using a dynamic Bayesian model averaging (DBMA) approach, the expectation-maximization method, and the ordinary Kriging interpolation method. The daily precipitation data merged using the DBMA approach exhibited distinct spatiotemporal variability, with an outstanding performance, as indicated by low root mean square error (RMSE=1.40 mm/d) and high Person's correlation coefficient (CC=0.67). Compared with the traditional simple model averaging (SMA) and individual product data, although the DBMA-fused precipitation data were slightly lower than the best precipitation product (CMFD), the overall performance of DBMA was more robust. The error analysis between DBMA-fused precipitation dataset and the more advanced Integrated Multi-satellite Retrievals for Global Precipitation Measurement Final (IMERG-F) precipitation product, as well as hydrological simulations in the Ebinur Lake Basin, further demonstrated the superior performance of DBMA-fused precipitation dataset in the entire Xinjiang region. The proposed framework for solving the fusion problem of multi-source precipitation data with different spatial resolutions is feasible for application in inland arid areas, and aids in obtaining more accurate regional hydrological information and improving regional water resources management capabilities and meteorological research in these regions.

Keywords: precipitation estimates; satellite-based and reanalysis precipitation; dynamic Bayesian model averaging; streamflow simulation; Ebinur Lake Basin; Xinjiang

Citation: XU Wenjie, DING Jianli, BAO Qingling, WANG Jinjie, XU Kun. 2024. Improving the accuracy of precipitation estimates in a typical inland arid area of China using a dynamic Bayesian model averaging approach. Journal of Arid Land, 16(3): 331–354. https://doi.org/10.1007/s40333-024-0054-7

*Corresponding author: DING Jianli (E-mail: dingjl@xju.edu.cn)
Received 2023-10-10; revised 2024-01-22; accepted 2024-01-29

1 Introduction

Precipitation plays a crucial role when examining worldwide shifts in climate patterns and intricate hydrological cycles (Ashouri et al., 2015; Rogelis and Werner, 2018; Kharaghani et al., 2023), and accurate and stable precipitation estimates are essential for weather monitoring, hydrological simulation, and surveillance and prevention of natural disasters (Yin et al., 2021; Tadesse et al., 2022). As the most reliable means for recording precipitation at specific locations, traditional ground-based precipitation measurement techniques (such as rain gauges and radar precipitation estimation) provide direct precipitation observations (Ur Rahman et al., 2019). However, influenced by diverse factors, such as topography, climatic conditions, and installation and operation costs, ground-based observations have limited spatial coverage and sparse and uneven distribution in certain regions (Lanza and Stagi, 2008; Yang et al., 2020), which seriously limits the understanding of actual precipitation over a wide spatial extent (Shen and Xiong, 2016). For example, one rain gauge is deployed over an area of about 1.58×10^4 km^2 in Xinjiang Uygur Autonomous Region, China with alternating mountainous-desert terrain and obvious spatial and temporal variability in precipitation, which leads to weak spatial representativeness of rain gauges, while interpolated spatially continuous precipitation data suffer from large errors, shifted precipitation centers, and irrational precipitation distributions (Katipoğlu, 2022). In recent years, with the advancement of remote sensing technology and reanalysis models, significant improvements have been made in addressing the spatiotemporal resolution challenges of traditional precipitation measurement networks, but there is regional variability among different precipitation datasets due to constraints imposed by data sources and algorithms (Gebregiorgis and Hossain, 2015; Muñoz-Sabater et al., 2021). Therefore, evaluating and integrating precipitation datasets from different sources to accurately characterize and understand regional precipitation patterns has become a challenge, as this approach can provide more accurate and alternative precipitation information for hydrological modelling in regions lacking information and may improve the performance of hydrological modelling in arid areas of Xinjiang.

To date, numerous precipitation products with high spatiotemporal resolution from both domestic and international sources have been made accessible to the public, including China Meteorological Forcing Dataset (CMFD) (He et al., 2020), Climate Prediction Center morphing method (CMORPH) (Joyce et al., 2004), Climate Hazards Group InfraRed Precipitation with Station (CHIRPS) (Funk et al., 2015), Tropical Rainfall Measuring Mission Multi-satellite Precipitation Analysis (TMPA) (Huffman et al., 2007), Precipitation Estimation from Remotely Sensed Information using Artificial Neural Networks-Climate Data Record (PERSIANN-CDR) (Hong et al., 2004), and ECMWF Reanalysis v5-Land Dataset (ERA5-Land) (Muñoz-Sabater et al., 2021). When constrained by various conditions, the global applicability of any precipitation product is limited, as its optimal performance is often confined to specific geographical regions. For instance, CHIRPS data show significant strengths and higher skill scores in daily, monthly, and yearly scale assessments in eastern Africa (Dinku et al., 2018), while TMPA exhibits better performance in recording extreme precipitation events in southern China (Wang et al., 2021). Moreover, differences in geographical location, elevation, and climatic conditions can result in spatial variations in precipitation products (Mosaffa et al., 2020; Bai et al., 2021; Wang et al., 2022). Tan and Santo (2018) reported that PERSIANN-CDR is unable to capture all precipitation categories in Malaysia by underestimating low precipitation levels and overestimating medium to heavy precipitation levels, while in the Huaihe River Basin of China, the dataset exhibits limited performance in capturing variations in extreme precipitation events (Sun et al., 2021). As mentioned earlier, the regional and temporal uncertainty of a single precipitation product may affect the quality of precipitation estimates and further limit the accuracy of hydrological simulations.

To address these questions, numerous researchers are dedicated to using various approaches to combine the diverse ground-based observations and satellite-based and reanalysis precipitation datasets to mitigate the uncertainties of individual members (Baez-Villanueva et al., 2020; Xu et

al., 2020; Yumnam et al., 2022). Research has indicated that data fusion integrates advantageous information from individual members to mitigate the limitations of singular data and exhibits superior performance compared to all or most independent precipitation estimates (Chen and Jahanshahi, 2018). The main precipitation data fusion approaches that are currently available include optimal interpolation (Wei et al., 2023b), data assimilation (Huffman et al., 2007), Bayesian model averaging (BMA) (Sloughter et al., 2007), and neural network analysis (Chen et al., 2018). Hoeting et al. (1998) proposed that linear combinations of models fail to correctly capture the strength of an individual model, while BMA approach can effectively balance the weights among multiple models and accurately consider uncertainty. The BMA approach integrates a predictive probability density function (PDF) from diverse models, with the predictive PDF of an individual variable represented as the weighted average of the posterior distribution of the model ensemble (Rings et al., 2012). To calculate the weights for each predictive variable, Raftery et al. (2005) utilized a machine learning algorithm (expectation-maximization) through iterative model parameter estimation to quantify the relative credibility of each model in interpreting the data, and applied it to the predictive PDFs of a developed meteorological forecast ensemble. In addition, Sloughter et al. (2007) used a single precipitation product to predict PDFs that exhibit a mixture of zero and gamma distributions, and successfully extended BMA to quantitatively forecast precipitation, leading to the applications of BMA to surface hydrology (Li and Tsai, 2009; Schöniger et al., 2014). Jiang et al. (2012) evaluated the applicability of three satellite-based precipitation datasets in the Mishui River Basin, China, by utilizing BMA to combine streamflow data from the Xin'anjiang model simulations and different precipitation products, which resulted in the merged streamflow exhibiting more robust performance. Ma et al. (2018) developed a dynamic Bayesian model averaging (DBMA) framework to optimize the relative weights of four satellite-based precipitation datasets over the Tibetan Plateau, China, confirming the superiority of DBMA ensemble over other conventional ensembles and individual members. Yumnam et al. (2022) presented the BMA approach that centered on different quantiles to train optimal weights for three precipitation products over the Vamsadhara River Basin along the Indian coast, demonstrating enhanced robustness in the performance of the fused precipitation dataset. The development of fusion algorithms is crucial for the utilization of precipitation integration schemes, and the choice of algorithms and input sources directly influences the performance of the fused precipitation dataset (Tang et al., 2020; Wei et al., 2023a). To effectively address the significant challenge of insufficient precipitation data in Xinjiang, we proposed a precipitation merging framework based on the DBMA approach and six satellite-based and reanalysis precipitation datasets over the region.

This study focused on (1) a detailed comparison of six widely used domestic and international high-resolution satellite-based and reanalysis precipitation datasets (CMORPH, CHIRPS, CMFD, PERSIANN-CDR, TMPA, and ERA5-Land) with rain gauge ground-based observations; (2) the utilization of DBMA approach to optimize combined precipitation data from six different sources to produce an ensemble multi-source precipitation dataset on a daily scale over the 1999–2018 time span to comprehensively evaluate its performance through a series of evaluation indicators and to compare it with the more advanced Integrated Multi-satellitE Retrievals for Global Precipitation Measurement Final (IMERG-F) product; and (3) a semi-distributed hydrological model to comprehensively assess the hydrological simulation performance of DBMA-fused precipitation and IMERG-F precipitation product in the Ebinur Lake Basin, Xinjiang. In this study, bilinear interpolation was employed to standardize the spatial resolution of multiple precipitation sources. The expectation-maximization algorithm was used to iterate the optimal weights of each fusion member at the ground meteorological stations. Finally, the point weights were spatially diffused to obtain continuous merged precipitation data via the ordinary Kriging interpolation method. The results of this research can effectively improve the accuracy of hydrological simulations in areas with missing precipitation data and enhance the effectiveness of regional water resources management in inland arid areas.

2 Study area and data sources

2.1 Study area

The Xinjiang Uygur Autonomous Region, China is located between 73°40′–96°18′E longitude and 34°25′–48°10′N latitude and is situated in the hinterland of the Eurasian Continent; its geographical area covers approximately one-sixth of the total land in China. Xinjiang has complex terrain characterized by an interplay of basins and mountain ranges, constituting a distinctive mountain-basin geomorphic system (Fig. 1). With the Altay Mountains on the northern boundary and the Kunlun Mountains on the southern boundary, the Tianshan Mountains in the middle are the natural geographical dividing line between the Junggar Basin and Tarim Basin. Xinjiang's topography exhibits significant differences in elevation and has obvious vertical climatic characteristics. The lowest elevation point occurs at the Aydingkol Lake (155 m below sea level) in the Turpan Basin, and the highest elevation point is at the Qogir Peak (8611 m above sea level). Although located in the northern temperate zone, Xinjiang is positioned far inland and distant from the sea, marking the culmination of atmospheric water vapour transport. Coupled with the obstruction of Indian Ocean moisture by the southern Tibetan Plateau, this leads to water vapour from the Atlantic Ocean becoming the primary moisture source for Xinjiang, as it is carried by the westerly circulation (Yin et al., 2017). In addition, the intercepting effect of high mountain ranges on westerly circulation and dry-cold moisture in the Arctic Ocean makes the arid mountainous areas of the region notable for their excess precipitation over the basin plains (Hu et al., 2021).

The spatial distribution of precipitation in Xinjiang is extremely uneven, with an average annual precipitation of only 157.7 mm. The northern region of Xinjiang receives more than 80% of the total annual precipitation, while the southern region of Xinjiang only receives less than 20%. Mountainous areas contribute 81% of Xinjiang's total annual precipitation, while plain regions (including desert and barren areas) receive only 19% (Zhang et al., 2022). As a typical inland river basin in Xinjiang, the Ebinur Lake Basin is characterized by low precipitation and high evaporation, and the basin's water resources are very sensitive to climate change.

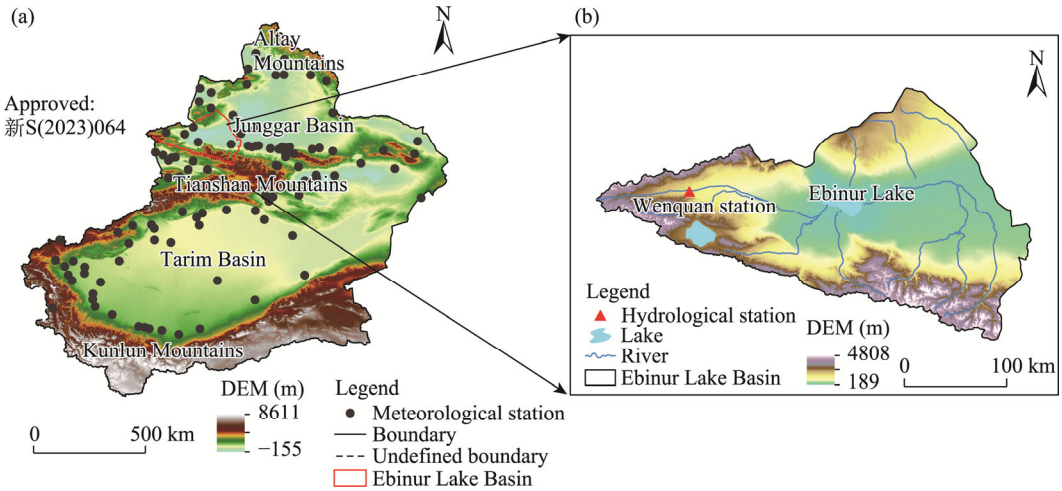

Fig. 1 Overview of Xinjiang Uygur Autonomous Region (a) and the Ebinur Lake Basin (b) based on the digital elevation model (DEM). Note that the figures are based on the standard map (新 S(2023)064) of the Map Service System (https://xinjiang.tianditu.gov.cn/main/bzdt.html) marked by the Xinjiang Uygur Autonomous Region Platform for Common Geospatial Information Services, and the standard map has not been modified.

2.2 Data

2.2.1 Ground-based observational precipitation data

The precipitation data from 105 ground meteorological stations distributed in Xinjiang used in this

study were sourced from the daily precipitation dataset of China's meteorological element observation sites available at the Resource and Environment Science and Data Center (https://www.resdc.cn/data.aspx?DATAID=230). This dataset comprises precipitation records from 26 national benchmark meteorological stations, 40 national basic meteorological stations, and 39 national general meteorological stations. All downloaded meteorological data underwent a sequence of quality control procedures, including formatting, internal consistency checks, elimination of duplicates, and identification and removal of anomalous data. The daily precipitation dataset refers to the accumulated precipitation within a 24-h period starting at 08:00 (Beijing time), which corresponds to Coordinated Universal Time (UTC) at 00:00. Therefore, the daily accumulated precipitation at the ground meteorological stations is temporally consistent with the precipitation product measured at 00:00 UTC.

Based on the temporal overlap period of meteorological observations and different precipitation product datasets, we defined the period in this study as 1999–2018. Additionally, the seasons mentioned in the paper followed the universally accepted Gregorian calendar standard for division. Specifically, spring is defined as the period from March to May, summer from June to August, autumn from September to November, and winter from December to February of the next year.

2.2.2 Satellite-based and reanalysis precipitation products

This study reviewed various satellite-based precipitation products (including CMORPH, CHIRPS, CMFD, PERSIANN-CDR, and TMPA) and the reanalysis precipitation dataset (ERA5-Land) to address the limited ground-based observation challenges in accurately estimating precipitation in data-scarce regions. In addition, the IMERG-F precipitation product was integrated with Global Precipitation Measurement (GPM), Tropical Rainfall Measuring Mission (TRMM), and other satellite-based data generated with a delay of approximately 2.5 months based on the monthly precipitation analysis of the Global Precipitation Climatology Centre (GPCC) product (Hou et al., 2014). This dataset provides high-quality precipitation estimates and is considered more suitable for scientific research (Wang et al., 2017). This paper compared the proposed method with DBMA-fused precipitation dataset in terms of independent site analysis and watershed simulation effectiveness. A further description of the precipitation products is provided in Table 1.

Table 1 General information of the precipitation products used in this study

Dataset	Spatial resolution	Temporal resolution	Coverage range	Period	Website
CHIRPS	0.05°	Daily	50°S–50°N	1981–present	https://www.chc.ucsb.edu/data/chirps
CMFD	0.10°	Daily	China (land only)	1979–2018	https://data.tpdc.ac.cn/zh-hans/data
CMORPH	0.25°	Daily	60°S–60°N	1998–present	https://climatedataguide.ucar.edu/climate-data
TMPA	0.25°	Daily	50°S–50°N	1998–2019	https://gpm.nasa.gov/data
PERSIANN-CDR	0.25°	Daily	60°S–60°N	1983–present	https://climatedataguide.ucar.edu/climate-data
ERA5-Land	0.10°	Hourly	Earth	1950–present	https://cds.climate.copernicus.eu
IMERG-F	0.10°	Hourly	Earth	2000–present	https://gpm.nasa.gov/data/imerg

Note: CHIRPS, Climate Hazards Group InfraRed Precipitation with Station; CMFD, China Meteorological Forcing Dataset; CMORPH, Climate Prediction Center morphing method; TMPA, Tropical Rainfall Measuring Mission Multi-satellite Precipitation Analysis; PERSIANN-CDR, Precipitation Estimation from Remotely Sensed Information using Artificial Neural Networks-Climate Data Record; ERA5-Land, ECMWF Reanalysis v5-Land; IMERG-F, Integrated Multi-satellitE Retrievals for Global Precipitation Measurement Final.

2.2.3 Other data sources

The recorded daily streamflow data from 2001 to 2014 at the Wenquan station in the Ebinur Lake Basin were provided by the Water Resources Department of Xinjiang Uygur Autonomous Region, China. Daily-scale meteorological forcing data for the period 2001–2014, including longwave and shortwave radiation, temperature, barometric pressure, and wind speed, were obtained from the China Meteorological Data Service Centre (http://data.cma.cn/), which are interpolated by the ordinary Kriging interpolation method. The soil-cover data were obtained from the Harmonized

World Soil Database (HWSD) developed by the International Institute for Applied Systems Analysis (IIASA) and the Food and Agriculture Organization of the United Nations (FAO). This study utilized the 2023 updated version of the HWSD (HWSD v.2.0) (https://gaez.fao.org/pages/hwsd). Vegetation-cover data for 1998 were obtained from the global land cover database developed by the University of Maryland, USA. The classification system for the UMD land cover data was designed for the Simple Biosphere Model (SIB) and was divided into a total of 14 land cover types.

3 Methods

3.1 Framework

Figure 2 shows the general process of the DBMA approach used to merge gridded precipitation data (including satellite-based and reanalysis precipitation datasets) with different spatial resolutions. The general process of merging gridded precipitation data used in this study was developed upon the algorithm introduced by Ma et al. (2018), which unifies gridded precipitation data with different spatial resolutions through a bilinear interpolation method, introduces a "discrete-continuous" hybrid model to describe the PDF of precipitation, and combines multiple gridded precipitation datasets using the DBMA approach.

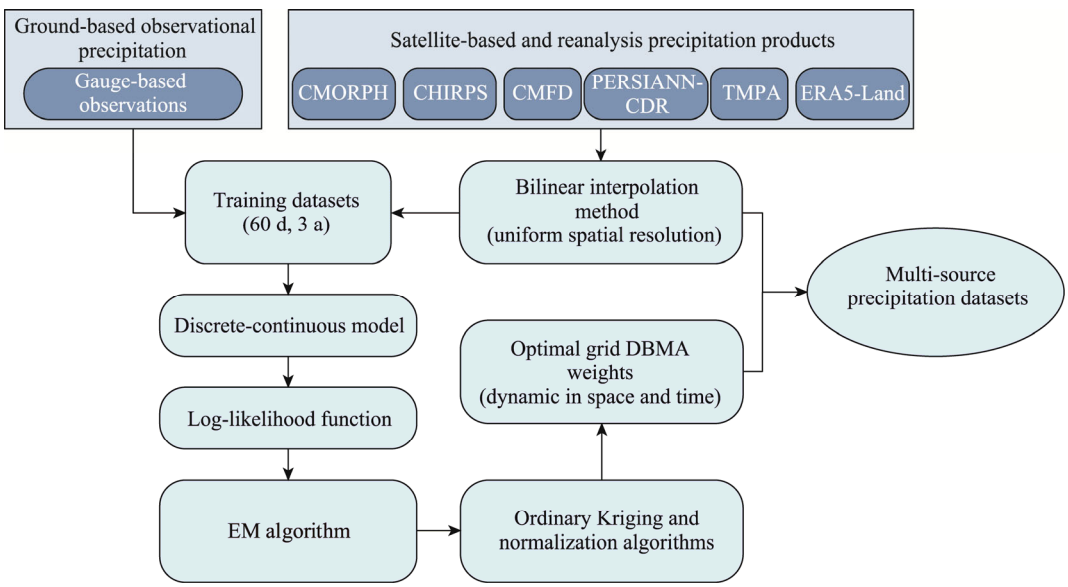

Fig. 2 Flowchart of the dynamic Bayesian model averaging (DBMA) approach for blending gridded precipitation data with different spatial resolutions. CHIRPS, Climate Hazards Group InfraRed Precipitation with Station; CMFD, China Meteorological Forcing Dataset; CMORPH, Climate Prediction Center morphing method; TMPA, Tropical Rainfall Measuring Mission Multi-satellite Precipitation Analysis; PERSIANN-CDR, Precipitation Estimation from Remotely Sensed Information using Artificial Neural Networks-Climate Data Record; ERA5-Land, ECMWF Reanalysis v5-Land; EM, Expectation-Maximization.

We established the estimation of model parameters based on training the model with simulated and observed data during the N days prior to model initialization. Previously, the training period used for weight estimation varied via DBMA approach. Sloughter et al. (2007) chose a month-long training duration to apply DBMA approach for 48 h forecasts over the North American Pacific region, while Ma et al. (2018) introduced a DBMA framework within a 40-d training timeframe to update the relative weights of four satellite-based precipitation datasets over the Tibetan Plateau region. Empirical evidence has shown that the training duration is strongly correlated with the specific conditions of the study area, and validation using actual data from the

study area is more reliable.

To evaluate the model training length, we calculated the root mean square error (RMSE) and Pearson's correlation coefficient (CC) for the DBMA dataset from precipitation data of 105 meteorological stations in Xinjiang in 2017, and compared these values across a range of potential training days (N=20, 25, 30, ..., 100). Figure 3 shows that the RMSE and CC initially exhibit downward and upward trends as the increase of training period length, respectively, and both of them reach their optimal values at 60 d. Beyond 60 d, the RMSE and CC demonstrate upward and downward trends, respectively, indicating deteriorating performance.

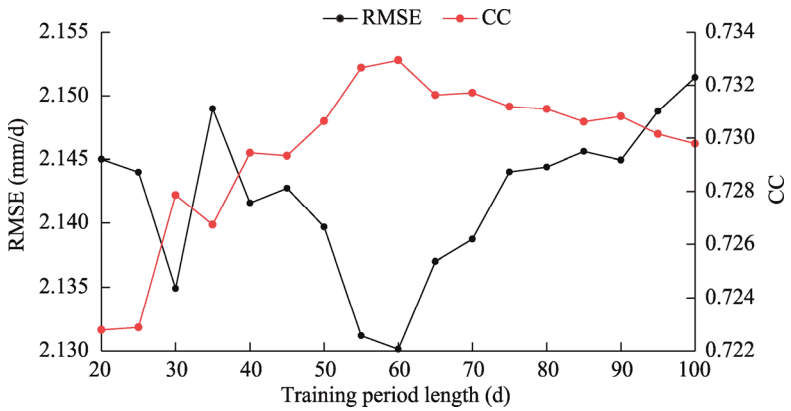

Fig. 3 Variations in the two indicators (RMSE and CC) between DBMA-based precipitation and ground-based observational precipitation data across different training period lengths. RMSE, root mean square error; CC, Pearson's correlation coefficient.

3.2 BMA technique

BMA is an ensemble technique in the fields of statistics and machine learning that combines forecasts and inferences from multiple competing models to generate more precise and dependable probabilistic combinations (Raftery et al., 2005). The BMA allocates weights to each model based on its posterior probability distribution during the training period, where the weight assigned is determined by how much each model quantifies the overall predictive likelihood.

The BMA approach is briefly described as follows. Assuming that the fused precipitation variable is y and the number of models is k, the prediction f_i of each ensemble member is associated with a conditional PDF $h_i(y \mid f_i)$ (the posterior distribution of y based on the training data of predictor i). Therefore, the PDF of fused precipitation variable y is calculated as follows:

$$p(y \mid f_1, f_2, \cdots, f_k) = \sum_{i=1}^{k} w_i h_i(y \mid f_i), \tag{1}$$

where $p(y \mid f_i)$ is the forecast PDF of the BMA ensemble y given the observed data; and w_i corresponds to the relative contribution of predictor i to the predicted variable during the training period, also known as the posterior probability of member i. To ensure that the ensemble prediction constitutes a complete probability distribution during the same training period, the sum of the posterior probabilities of the members is equal to 1.

Raftery et al. (2005) applied a deviation correction-centered normal distribution to fit the conditional PDF of variables, such as temperature and sea-level pressure. However, for cumulative precipitation distribution data, the value equals to zero in most cases, and for the part that does not equal to zero, the distribution is highly skewed; therefore, the normal distribution is not suitable for precipitation data. To extend BMA to precipitation variables, Sloughter et al. (2007) proposed a hybrid model based on discrete continuous component distributions for BMA modelling, where the conditional PDF of the ensemble members corresponds to a mixture of discrete components at zero

and gamma distributions. This model was successfully applied to the daily forecast of 24 h cumulative precipitation over the Pacific Northwest of North America through a mesoscale ensemble at the University of Washington, USA.

In the standard BMA used by Raftery et al. (2005), the conditional PDF $p(y \mid f_i)$ (Eq. 1) is usually approximated using the normal distribution centered on a linear function, while in the mixed model with the "discrete-continuous" component distribution proposed by Sloughter et al. (2007), the conditional PDF for the precipitation variable is expressed as follows:

$$p(y_0 \mid f_1, f_2, \cdots, f_k) = \sum_{i=1}^{k} w_i [p(y_0 = 0 \mid f_i) I[y_0 = 0] + p(y_0 > 0 \mid f_i) g_i(y_0 \mid f_i) I[y_0 > 0]], \quad (2)$$

where y_0 is the cube root of cumulative precipitation; and the general indicator function $I[y_0=0]$ or $I[y_0>0]$ is unity if the condition in brackets holds, otherwise it is zero. The term $p(y_0 = 0 \mid f_i)$ is specified by Equation 3. The conditional PDF $g_i(y_0 \mid f_i)$ of precipitation amount y_0 given that it is positive is a gamma distribution with PDF.

$$logitp(y_0 = 0 \mid f_i) = a_{0i} + a_{1i} f_i^{1/3} + a_{2i} \delta_i, \quad (3)$$

$$g_i(y_0 \mid f_i) = \frac{1}{\beta_i^{\alpha_i} \Gamma(\alpha_i)} y_0^{\alpha_i - 1} \exp(-y_0 / \beta_i), \quad (4)$$

where *logit* is a logit function; a_{0i}, a_{1i}, and a_{2i} are parameters, which are determined by logistic regression using precipitation (or zero precipitation) as the dependent variable and $f_i^{1/3}$ and δ_i as the predictor variables; if f_i=0, δ_i is equal to 1, otherwise it is equal to 0; and Γ is the gamma function. The parameters $\alpha_i = \mu_i^2 / \sigma_i^2$ and $\beta_i = \sigma_i^2 / \mu_i$ of the gamma distribution are depended on f_i through the following relationships:

$$\mu_i = b_{0i} + b_{1i} f_i^{1/3}, \quad (5)$$

$$\sigma_i^2 = c_0 + c_1 f_i, \quad (6)$$

where μ_i and σ_i^2 are the mean and the variance of the distribution, respectively. The parameters b_{0i} and b_{1i} are determined by linear regression, and the parameters c_0 and c_1 are estimated by the maximum likelihood technique from the training data.

3.3 Performance evaluation

In this study, several common statistical indicators were utilized to quantitatively evaluate the performances of different satellite-based and reanalysis precipitation products and merged precipitation datasets in terms of precipitation estimation. Evaluation indicators of CC, RMSE, and relative bias (RB) were used to assess the consistency between the estimated and observed precipitation data. The mean absolute error (MAE), Kling-Gupta efficiency (KGE), and Theil's U statistic were utilized to measure the average error, similarity, and disparity, respectively, between the estimated and observed precipitation data. Additionally, the ability of the gridded precipitation datasets to detect precipitation was evaluated using the following three indicators: the probability of detection (POD) to measure the ability of precipitation product to detect the actual precipitation events, the false alarm rate (FAR) to represent the proportion of incorrectly predicted precipitation events according to the estimated precipitation, and the critical success index (CSI) to gauge the overall accuracy of the estimated precipitation in predicting precipitation. The optimal scores for POD and CSI are both 1.00, while the optimal score for FAR is 0.00; moving towards these optimal scores indicates more satisfactory estimation results. Furthermore, the Nash-Sutcliffe efficiency (NSE) was utilized to quantitatively assess the ability of the variable infiltration capacity (VIC) model to simulate streamflow. The formula and optimal values of the above indicators are shown in Table 2.

Table 2 Equations and optimal values of the evaluation indicators used in this study

Evaluation indicator	Equation	Optimal value
Mean absolute error (MAE; mm/d)	$\mathrm{MAE}=\frac{1}{n}\sum_{j=1}^{n}\left\|M_j-G_j\right\|$	0
Pearson's correlation coefficient (CC)	$\mathrm{CC}=\frac{\sum_{j=1}^{n}\left(M_j-\overline{M}\right)\left(G_j-\overline{G}\right)}{\sqrt{\sum_{j=1}^{n}\left(M_j-\overline{M}\right)^2}\sqrt{\sum_{j=1}^{n}\left(G_j-\overline{G}\right)^2}}$	1
Root mean square error (RMSE; mm/d)	$\mathrm{RMSE}=\sqrt{\frac{1}{n}\sum_{j=1}^{n}\left(M_j-G_j\right)^2}$	0
Relative bias (RB; %)	$\mathrm{RB}=\frac{\sum_{j=1}^{n}\left(M_j-G_j\right)}{\sum_{j=1}^{n}G_j}\times 100\%$	0
Theil's U (μ)	$\mu=\sqrt{\sum_{j=1}^{n}\left(M_j-G_j\right)^2/\sum_{j=1}^{n}M_j^2}$	0
Kling-Gupta efficiency (KGE)	$\mathrm{KGE}=1-\sqrt{(\mathrm{CC}-1)^2+(\beta-1)^2+(\gamma-1)^2}$ where $\beta=\overline{M}/\overline{G}$, $\gamma=\mathrm{CV}_M/\mathrm{CV}_G$	1
Critical success index (CSI)	$\mathrm{CSI}=\frac{H}{H+T+F}$	1
Probability of detection (POD)	$\mathrm{POD}=\frac{H}{H+T}$	1
False alarm rate (FAR)	$\mathrm{FAR}=\frac{F}{H+F}$	0
Nash-Sutcliffe efficiency (NSE)	$\mathrm{NSE}=1-\frac{\sum_{j=1}^{n}\left(S_{sim}-S_{obs}\right)^2}{\sum_{j=1}^{n}\left(S_{obs}-\overline{S_{obs}}\right)^2}$	1

Note: n is the number of samples; M_i and G_i are the estimated and observed precipitation data, respectively; $\overline{M}$ and $\overline{G}$ are the mean of estimated precipitation data and the mean of observed precipitation data, respectively; CV_M and CV_G are the coefficients of variation of estimated and observed precipitation data, respectively; β is the mean ratio between estimated and observed values; γ is the variance ratio between estimated and observed values; H is the number of observed precipitation events simultaneously monitored by the evaluated precipitation products; T is the number of observed precipitation events that were not monitored by the evaluated precipitation products; F is the number of "unobserved" precipitation events monitored by the evaluated precipitation products; S_{sim} and S_{obs} are the simulated and observed streamflow, respectively; and $\overline{S_{obs}}$ is the average of the observed streamflow values.

To evaluate the developed DBMA dataset, we further used traditional ensemble method (simple model averaging (SMA)) for intercomparison. The SMA scheme assigns the same weight to all members, i.e., the arithmetic mean of all individuals, which is calculated as follows:

$$R=\frac{1}{m}\sum_{\mathrm{d}=1}^{m}Q_d\ , \tag{7}$$

where R (mm) is the mixed precipitation data using the SMA method; m is the number of precipitation products; and Q_d is the combined ensemble members.

4 Results

4.1 Accuracy evaluation of multi-source precipitation datasets

Table 3 displays the comparison of daily precipitation between the six satellite-based and reanalysis precipitation products and ground-based observational precipitation data from 1999 to 2018. The results indicated that CMFD exhibited the highest correlation with observed precipitation (CC=0.62), followed by ERA5-Land (CC=0.55), and the remaining four

precipitation products exhibited comparatively lower accuracy (CCs between 0.25 and 0.28). The correlation of satellite-based and reanalysis precipitation products at meteorological stations was visually represented with greater precision in spatial presentation, where values in the northern region of the study area were generally higher than those in the southern region (Fig. 4). In terms of RB, the products of CMFD, CHIRPS, and TMPA slightly underestimated the actual precipitation, while the remaining three precipitation products had different degrees of overestimation (Table 3). The CMFD had the best agreement with real precipitation (RB= –0.11%), while ERA5-Land dataset strongly overestimated the daily precipitation in Xinjiang (RB=34.46%). The estimated daily precipitation for all the satellite-based and reanalysis precipitation datasets exhibited similar error sizes, ranging from 1.78 to 2.73 mm/d according to the RMSE statistical indicator.

Table 3 Statistical evaluation of the daily precipitation for the six satellite-based and reanalysis precipitation products compared with the ground-based observational precipitation data during 1999–2018

Statistic	CHIRPS	CMORPH	CMFD	PERSIANN-CDR	TMPA	ERA5-Land
CC	0.27	0.25	0.62	0.28	0.28	0.55
RMSE (mm/d)	2.58	2.73	1.78	2.16	2.38	2.00
RB (%)	–0.96	11.87	–0.11	16.07	–5.08	34.46
POD	0.33	0.45	0.83	0.71	0.40	0.92
FAR	0.67	0.62	0.58	0.70	0.61	0.72
CSI	0.20	0.26	0.39	0.26	0.25	0.27

Furthermore, this research assessed the accuracy of the six satellite-based and reanalysis precipitation products in terms of daily precipitation in various seasons (Table 4). Overall, the correlation between the satellite-based and reanalysis precipitation products and ground-based observational precipitation data in summer (CCs: 0.24–0.67) was better than those in autumn (CCs: 0.23–0.63), spring (CCs: 0.15–0.60), and winter (CCs: 0.01–0.64). The correlations and errors between CMFD precipitation product and observed precipitation in spring, summer, and autumn were optimal, with slight overestimation (or underestimation) of the actual daily precipitation, while CMFD precipitation product exhibited significant overestimation in winter (RB=9.94%). In addition, ERA5-Land exhibited the best correlation (CC=0.64) and lowest error (RMSE=0.86 mm/d) with the observed precipitation in winter, and the overestimation of the actual daily precipitation persisted throughout the year, with spring and autumn being the most severe. Notably, the CC of CMORPH was only 0.01 in winter, indicating a basic lack of correlation with ground-based observational precipitation and exhibiting the highest degree of underestimation (RB= –44.47%) in actual precipitation, which aligned with the finding of Guo et al. (2017) that CMORPH was unsuitable as an alternative dataset for regions covered by ice and snow. The RMSE indicator of estimated precipitation based on the satellite-based and reanalysis precipitation products exhibited distinct seasonal variations in the level of dispersion between estimated and observed data. The average RMSE values for all products across different seasons ranking from the highest to lowest were 3.04 mm/d in summer, 2.32 mm/d in spring, 1.97 mm/d in autumn, and 1.35 mm/d in winter.

To accurately assess the performance of daily precipitation data estimated from different datasets for precipitation detection, we compiled the POD, FAR, and CSI for different precipitation datasets in this paper. Table 4 showed that CMFD had the best performance in detecting precipitation and non-precipitation days, with a CSI value of 0.39, and CHIRPS had the worst detection capability (CSI=0.20). The spatial distribution of CSI metric (Fig. 4) showed a clear dividing line in the Tianshan Mountains, where the southern region of the study area exhibited lower CSI values than the northern region. In addition, the spatial distribution of POD at the meteorological stations clearly showed that the values of ERA5-Land, CMFD, and PERSIANN-CDR were significantly greater than those of the remaining three precipitation

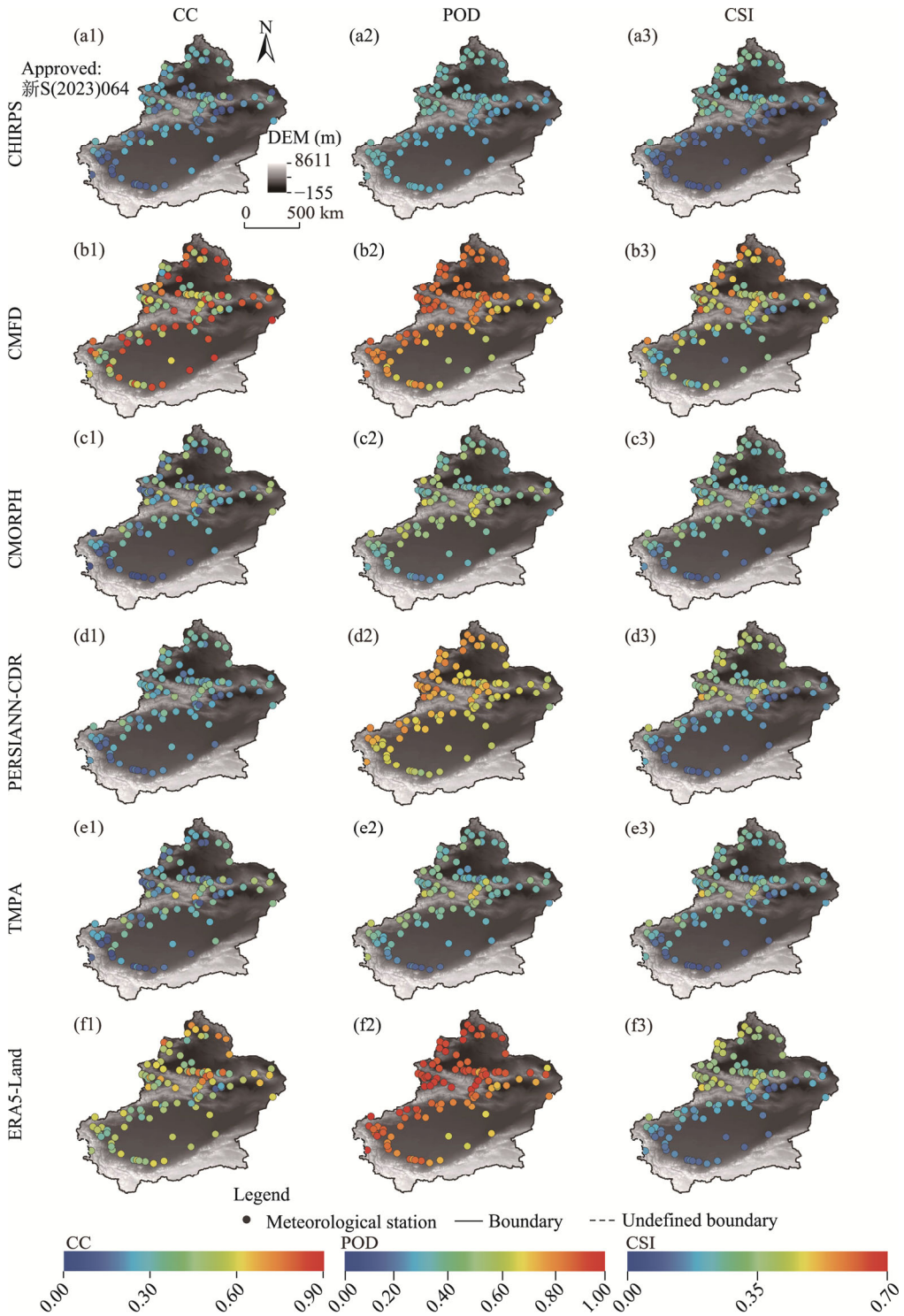

Fig. 4 Spatial distributions of the statistical indicators (CC, POD, and CSI) for CHIRPS (a1–a3), CMFD (b1–b3), CMORPH (c1–c3), PERSIANN-CDR (d1–d3), TMPA (e1–e3), and ERA5-Land (f1–f3) precipitation products at 105 meteorological stations in Xinjiang during 1999–2018. POD, probability of detection; CSI, critical success index; CHIRPS, Climate Hazards Group InfraRed Precipitation with Station; CMFD, China Meteorological Forcing Dataset; CMORPH, Climate Prediction Center morphing method; PERSIANN-CDR, Precipitation Estimation from Remotely Sensed Information using Artificial Neural Networks-Climate Data Record; TMPA, Tropical Rainfall Measuring Mission Multi-satellite Precipitation Analysis; ERA5-Land, ECMWF Reanalysis v5-Land.

Table 4 Statistical evaluation of the six satellite-based and reanalysis precipitation products compared with observed precipitation data in different seasons during 1999–2018

Season	Statistic	CHIRPS	CMORPH	CMFD	PERSIANN-CDR	TMPA	ERA5-Land
Spring	CC	0.31	0.15	0.60	0.29	0.23	0.57
	RMSE (mm/d)	2.36	3.18	1.80	2.12	2.46	2.03
	RB (%)	4.50	25.13	–3.51	4.81	–17.21	48.36
	POD	0.45	0.46	0.81	0.77	0.38	0.91
	FAR	0.70	0.67	0.59	0.73	0.62	0.74
	CSI	0.22	0.24	0.37	0.25	0.23	0.26
Summer	CC	0.24	0.36	0.67	0.25	0.37	0.50
	RMSE (mm/d)	3.82	3.27	2.27	3.04	2.97	2.85
	RB (%)	–5.59	20.09	–2.28	18.39	2.67	19.03
	POD	0.21	0.72	0.87	0.76	0.63	0.93
	FAR	0.45	0.55	0.57	0.63	0.54	0.66
	CSI	0.18	0.38	0.40	0.33	0.36	0.33
Autumn	CC	0.27	0.23	0.63	0.30	0.24	0.58
	RMSE (mm/d)	2.25	2.33	1.54	1.87	2.11	1.74
	RB (%)	2.68	10.58	2.83	18.57	–16.48	50.48
	POD	0.31	0.44	0.80	0.71	0.34	0.89
	FAR	0.63	0.67	0.61	0.71	0.65	0.75
	CSI	0.20	0.23	0.36	0.26	0.21	0.24
Winter	CC	0.31	0.01	0.40	0.27	0.13	0.64
	RMSE (mm/d)	1.07	1.87	1.35	1.12	1.82	0.86
	RB (%)	–3.17	–44.47	9.94	28.55	14.64	29.90
	POD	0.38	0.02	0.80	0.57	0.14	0.92
	FAR	0.75	0.90	0.52	0.76	0.75	0.75
	CSI	0.18	0.02	0.43	0.20	0.10	0.25

product, and the spatial distribution of POD values was relatively uniform, with no high-value concentration areas. FAR analysis implied that CMFD could detect 58% of the erroneous precipitation events, and the FARs of the remaining products were all higher than 0.60, with the highest value occurring in the ERA5-Land dataset, where 72% of the precipitation events were unobservable by the rain gauges (Table 3). Table 4 reveals that in summer, the best precipitation event occurrence for all precipitation products is approximately 0.33 on average, with CMFD and CMORPH having 0.40 and 0.38, respectively. On the other hand, winter is the season with the lowest occurrence of precipitation events (indicated by CSI) and the highest estimation error (indicated by FAR), with averages of 0.20 and 0.74, respectively. The best performer in winter was CMFD, with CSI and FAR values of 0.43 and 0.52, respectively, while CMORPH performed the worst in this season, with an FAR of 0.90 and a CSI of only 0.02.

4.2 Distribution model of DBMA-fused precipitation weights

Figure 5 shows the distribution of the average relative weights of the combined members of the DBMA-fused precipitation during 1999–2018. The CMFD and ERA5-Land members were assigned higher relative weights, with average values of 0.57 and 0.38, respectively. The remaining members exhibited lower relative weight assignments, with CMORPH having an

average relative weight value of 0.02, while CHIRPS, PERSIANN-CDR, and TMPA maintained the average relative weights of approximately 0.01. Differential weight allocations among distinct members were most obvious in terms of seasonal variations. The combined CMFD and ERA5-Land members exhibited comparable relative weight distributions during the winter and spring seasons but greater disparities during the summer and autumn seasons. The most pronounced discrepancy occurred around the end of the summer season, during which time the CMORPH member reached its peak in multi-year average relative weight. The relative weight allocations for the other combined members showed minimal fluctuations throughout the year, generally remaining within the range of 0.00–0.02.

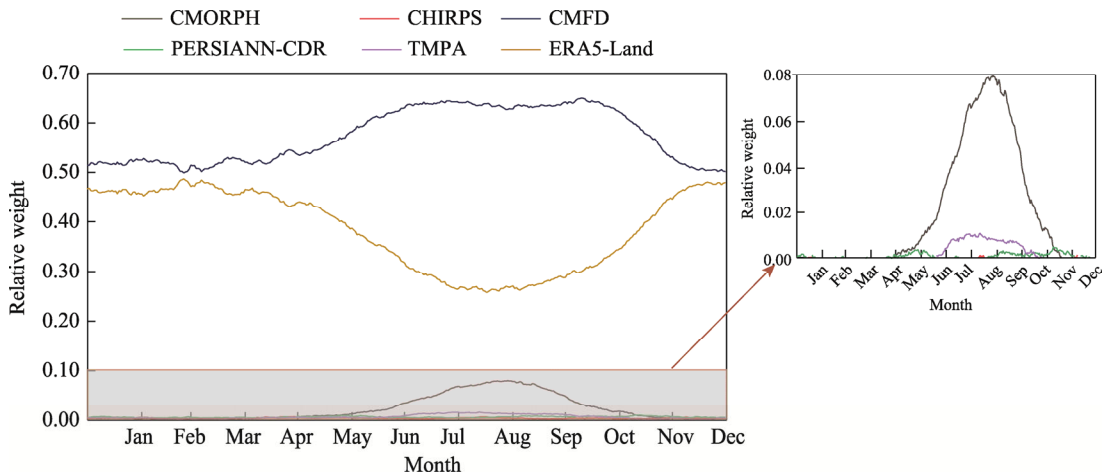

Fig. 5 Distributions of the multi-year monthly average relative weights of the six satellited-based and reanalysis precipitation products (CHIRPS, CMFD, CMORPH, PERSIANN-CDR, TMPA, and ERA5-Land) during 1999–2018

Figure 6 exhibits the average relative weights of the six satellited-based and reanalysis precipitation products in different seasons during 1999–2018, facilitating the analysis of the seasonal weight variations in the combined members. Overall, the proportions of average relative weights assigned to different members by DBMA were generally consistent in different seasons. Specifically, CMFD and REA5-Land received higher average relative weights; the sum of which was as high as approximately 0.90, while the total relative weight distribution of the remaining members was approximately 0.10. In addition, varying average relative weights among different members were evident in different seasons.

In spring and winter, CMFD exhibited a relatively uniform distribution of average relative weights, ranging from 0.02 to 0.90, with a mean of approximately 0.50. The average relative weight distribution of ERA5-Land ranged from 0.10 to 0.95, with a mean of approximately 0.40. The average relative weight distributions of the other members generally remained below 0.20, with a mean of approximately 0.02. In summer and autumn, the average relative weight distribution of CMFD ranged from 0.10 to 0.90, with a mean of approximately 0.60, while that of REA5-Land varied from 0.02 to 0.80, with a mean of approximately 0.30. In comparison to the spring and winter seasons, DBMA assigned higher average relative weights to the member CMFD in summer and autumn, and REA5-Land had a comparatively weaker performance. In addition, CHIRPS received extremely low average relative weight allocations during the summer and autumn seasons, with a mean of approximately 0.01, rendering it essentially negligible. Results of CMORPH indicated that some rain gauge stations had an average relative weight distribution between 0.20 and 0.40, with a mean of approximately 0.06 in summer and autumn, which implied a significant improvement in performance compared with those in the other two seasons.

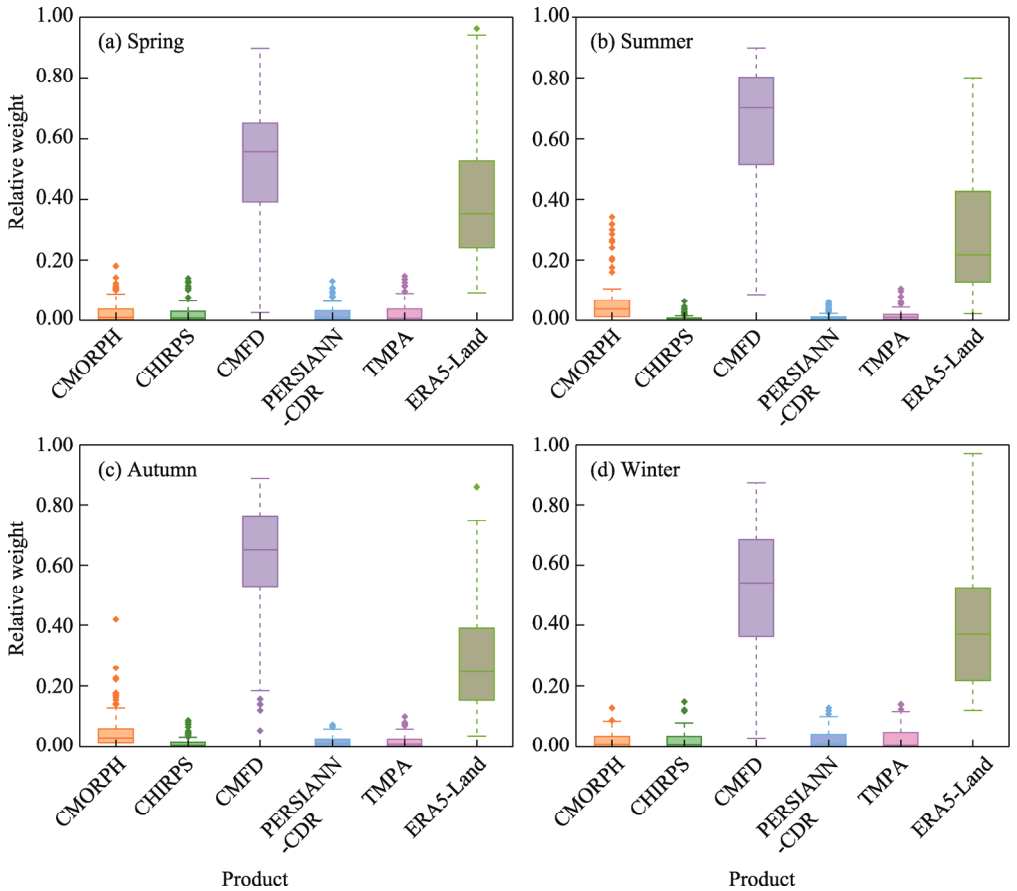

Fig. 6 Average relative weights of the six satellited-based and reanalysis precipitation products (CHIRPS, CMFD, CMORPH, PERSIANN-CDR, TMPA, and ERA5-Land) used for DBMA calculations in different seasons during 1999–2018. (a), spring; (b), summer; (c), autumn; (d), winter. Dots indicate data points of average relative weights. Box boundaries indicate the 25th and 75th percentiles, and whiskers below and above the box indicate the 10th and 90th percentiles, respectively. The black horizontal line within each box indicates the median of data points.

4.3 Statistical evaluation and comparison of DBMA-fused precipitation data

Figure 7 represents the spatial distribution of evaluation indicators for DBMA-fused precipitation at the grid scale in Xinjiang, with all assessments ensuring the presence of at least one rain gauge station within the grid scale. Overall, the performance of DBMA-fused precipitation data was satisfactory compared with the ground-based observational daily precipitation data in Xinjiang, with an overall CC of 0.67 (Fig. 7b); additionally, the areas with higher CC values were located around the Tianshan Mountains, Altay Mountains, and Kunlun Mountains, where alpine melting ice and high mountain ranges created favorable conditions for precipitation in the surrounding areas. The RMSE of DBMA-fused precipitation data decreased sequentially from the Tianshan Mountains to the northern and southern regions of Xinjiang, ranging from 4.20 to 0.34 mm/d, with a mean value of 1.40 mm/d for the whole Xinjiang region (Fig. 7a). According to the RB indicator, the mean value in Xinjiang was 21.5%, and the overestimation of precipitation was mainly distributed around the Tianshan Mountains and the southwestern region of Xinjiang, where precipitation was more abundant than in other regions; moreover, the underestimation mainly occurred in the southeastern and northern regions of Xinjiang, most of which were located around the two deserts: Taklimakan Desert and Kumtag Desert (Fig. 7c). Finally, DBMA-fused precipitation exhibited higher POD with a mean value of 0.92 (Fig. 7d), and its spatial distribution increased gradually from the southeast to northwest of Xinjiang, with a particular advantage in

the Tianshan Mountains, indicating that DBMA approach contributed to enhancing the spatial detecting capability of precipitation. Based on the aforementioned statistical indicators, the quality of DBMA-fused precipitation data in Xinjiang was basically acceptable at the daily scale during 1999–2018.

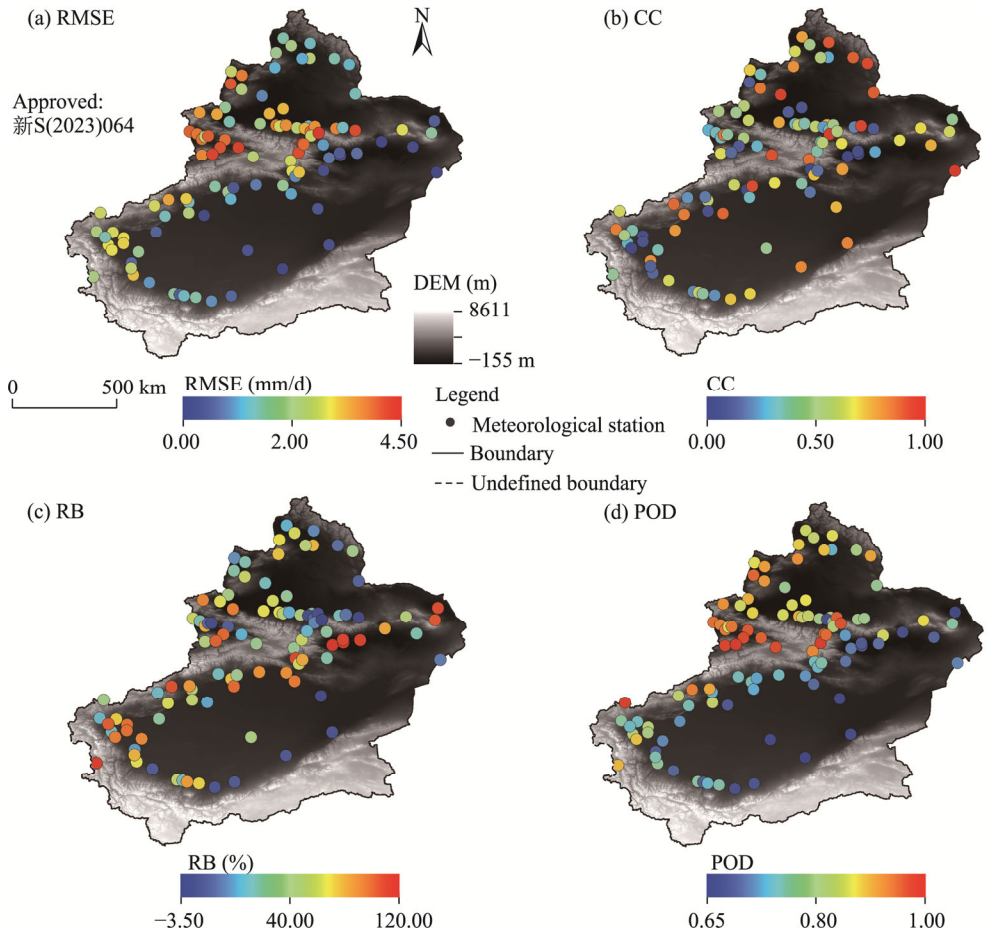

Fig. 7 Spatial distributions of RMSE (a), CC (b), RB (c), and POD (d) of DBMA-fused precipitation data at 105 meteorological stations in Xinjiang during 1999–2018. RB, relative bias.

To further quantify the performance of DBMA in Xinjiang, we selected six evaluation indicators to compare and assess the daily precipitation from two ensembles (DBMA-fused precipitation and SMA-based precipitation) and six satellite-based and reanalysis precipitation products at 105 meteorological stations (Table 5). The ensemble SMA has an advantage over the other merged members except for CMFD, especially in the POD, mainly because SMA assigns the same weight to the merged members and the ensemble apparently captures more precipitation events than the individual merged members. More importantly, DBMA significantly outperforms SMA and most individual merged members. Compared with the best merged member (i.e., CMFD), DBMA yielded improvement rates of 2.17%, 7.46%, 21.35%, 9.78%, and 6.45% in terms of MAE, CC, RMSE, POD, and Theil's U, respectively. The rates of improvement of DBMA compared with the poorest performing members of the indicators were 41.56%, 59.70%, 48.72%, 64.13%, and 45.96%, respectively, for MAE, CC, RMSE, POD, and Theil's U. Notably, the KGE score of DBMA was 0.56, which was slightly lower than that of the best member (CMFD); however, DBMA had significant advantages over other individual merged members. Thus, in contrast to the individual merged members and the ensemble SMA, DBMA showed

better overall performance in terms of evaluation indicators. The results emphasized the practicability of utilizing DBMA to fuse satellite-based and reanalysis precipitation datasets in the study area.

Table 5 Evaluation indicators of daily precipitation from two ensembles (DBMA-fused precipitation and SMA-based precipitation) and six satellite-based and reanalysis precipitation products at 105 meteorological stations in Xinjiang

Ensemble/member	MAE (mm/d)	CC	RMSE (mm/d)	POD	KGE score	Theil's U
DBMA	0.45#	0.67#	1.40#	0.92	0.56	0.87#
SMA	0.59	0.55	1.80	0.97#	0.35	1.30
CHIRPS	0.72	0.27	2.58	0.33	0.27	1.19
CMORPH	0.77	0.25	2.73	0.45	0.24	1.16
CMFD	0.46	0.62	1.78	0.83	0.59#	0.93
PERSIANN-CDR	0.76	0.28	2.16	0.71	0.10	1.61
TMPA	0.70	0.28	2.38	0.40	0.27	1.29
ERA5-Land	0.62	0.55	2.00	0.92	0.36	0.93

Note: DBMA, dynamic Bayesian model averaging; SMA, simple model averaging. # represents the best score for the compared ensembles and members.

According to the spatial patterns of multi-year average precipitation from the eight precipitation datasets (two ensembles and six satellite-based and reanalysis precipitation products) during the period 1999–2018 (Fig. 8), the overall trend of multi-year average precipitation decreased from the northwest to southeast of Xinjiang. The areas with lower precipitation were located in the southern region of Xinjiang and were occupied by the Taklimakan Desert, while relatively abundant precipitation was found in the higher altitude regions of the Tianshan Mountains, Altay Mountains, and the narrow central part of the Kunlun Mountains. These findings also indicated that the geographical distribution characteristics of precipitation in Xinjiang were closely related to altitude. Nevertheless, different datasets exhibited pronounced disparities in the spatial pattern of multi-year average precipitation. For CHIRPS dataset, the precipitation-rich regions are concentrated in the foothills of the Tianshan Mountains and the Ili River Valley, where precipitation reaches approximately 800–1000 mm, with some areas on the northern slopes of the Tianshan Mountains as high as 1200 mm, which is severely overestimated in some regions. For CMORPH and TMPA products, the spatial patterns of multi-year average precipitation lacked continuity, with inherent product characteristics resulting in the significant presence of outliers in regions with water bodies (Tang et al., 2016). In comparison to the latter, the former provided a more abundant estimate of multi-year average precipitation in the Kunlun Mountains and a worse estimate of multi-year average precipitation in the Ili River Valley. The PERSIANN-CDR dataset contained the highest multi-year average precipitation in the western region of Xinjiang, with a gradual decrease from the west to east in a circular pattern, which did not align with the actual conditions. The multi-year average precipitation distributions of CMFD, ERA5-Land, SMA, and DBMA all exhibited the spatial patterns of "high in the north and low in the south", with higher precipitation levels occurring near the high-altitude Tianshan Mountains, Altay Mountains, and Kunlun Mountains. The overall low precipitation area of the Tarim Basin extending eastwards to the Turpan-Hami Basin was basically consistent with the actual precipitation profile of Xinjiang. However, ERA5-Land product significantly overestimated multi-year average precipitation on the northern and southern slopes of the Tianshan Mountains and the Ili River Valley, reaching up to approximately 1700 mm in some regions, indicating substantial deviation from actual precipitation.

4.4 Comparison of DBMA-fused precipitation dataset with the latest IMERG-F precipitation product

Error analysis of 105 meteorological stations revealed that DBMA outperformed IMERG-F for all the evaluation indicators in Xinjiang (Table 6). Specifically, DBMA-fused precipitation dataset

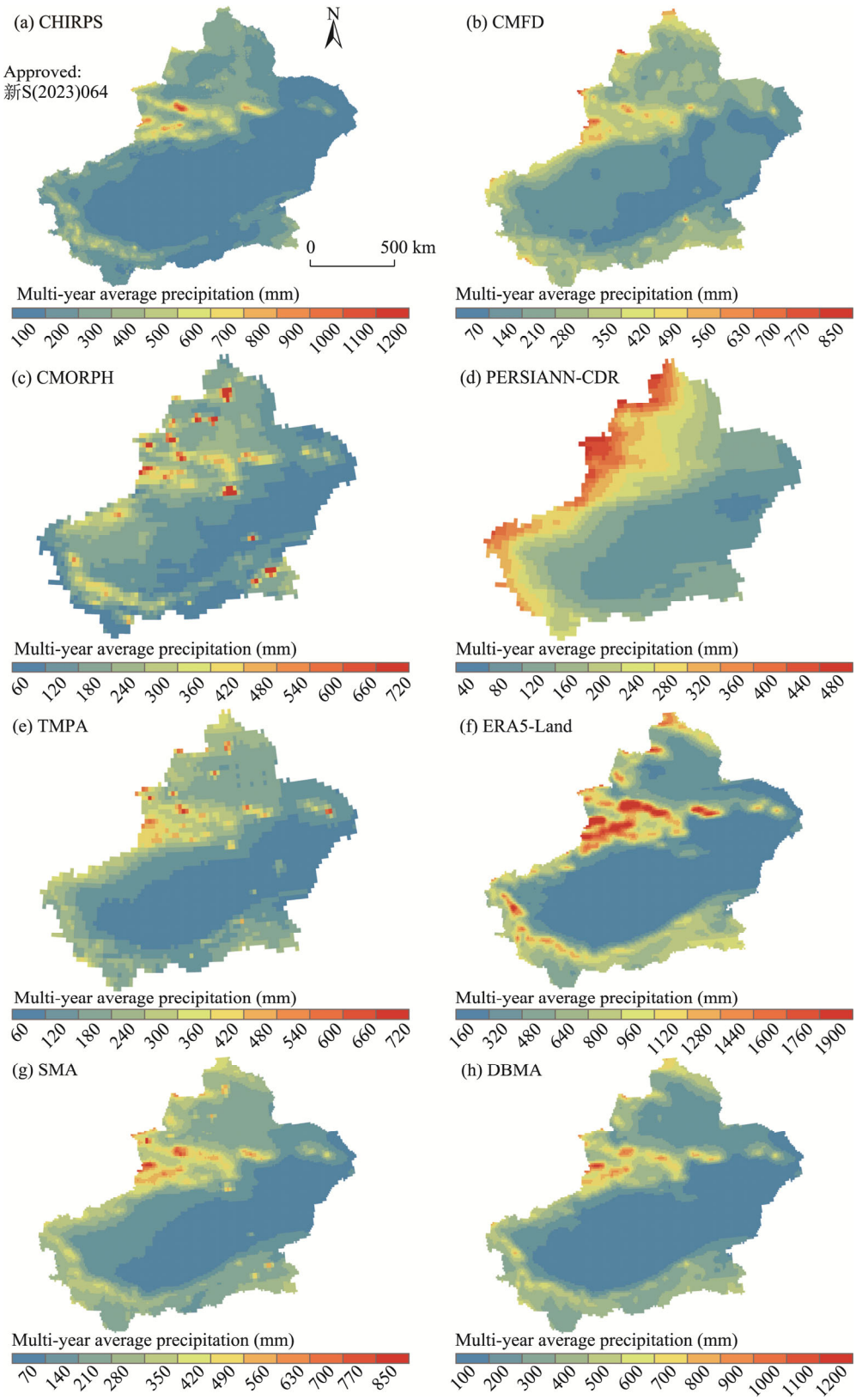

Fig. 8 Spatial distributions of multi-year average precipitation in Xinjiang during 1999–2018 based on CHIRPS (a), CMFD (b), CMORPH (c), PERSIANN-CDR (d), TMPA (e), ERA5-Land (f), SMA (g), and DBMA (h). SMA, simple model averaging.

Table 6 Daily-scale evaluation indicators of DBMA-fused precipitation dataset and the latest IMERG-F product at 105 meteorological stations in Xinjiang during 2001–2014

Dataset	MAE (mm/d)	CC	RMSE (mm/d)	POD	KGE score	Theil's U
DBMA	0.55#	0.65#	1.79#	0.87#	0.54#	0.93#
IMERG-F	0.71	0.42	2.28	0.68	0.38	1.16

Note: # represents the best score for the compared datasets.

showed lower MAE, RMSE, and Theil's U values, with improvements of 22.97%, 21.52%, and 19.90%, respectively, over the IMERG-F precipitation product. The CC and KGE indicators of DBMA-fused precipitation dataset were the most satisfactory, with improvements of 34.86% and 29.20%, respectively, compared with the IMERG-F precipitation product. In addition, DBMA significantly improved the actual precipitation event detection, with a POD of 0.87. Preliminary comparisons with this product indicated that the accuracy of the developed DBMA-fused precipitation dataset was acceptable for a multi-source satellite precipitation product in Xinjiang.

For a more comprehensive evaluation of the hydrological utility of DBMA-fused precipitation dataset in the Ebinur Lake Basin, Xinjiang, this research utilized two distinct precipitation datasets (DBMA-fused precipitation dataset and IMERG-F precipitation product) as control variables for streamflow simulation via the VIC model. Figure 9 shows a comparison of the reproduced monthly streamflow based on these two precipitation datasets for hydrological simulations at the Wenquan station in the Ebinur Lake Basin during 2001–2014. The results showed that the VIC model-simulated streamflow driven by the two precipitation datasets followed the same trend as the observed streamflow and was able to capture most of the streamflow peaks. DBMA-fused precipitation simulated streamflow better in summer than in winter, when actual streamflow tended to be overestimated and fluctuated erratically. The IMERG-F-simulated streamflow was greater than the observed streamflow throughout the study period (2001–2014), with more pronounced fluctuations occurring in winter. Compared with the IMERG-F-simulated streamflow, the DBMA-fused precipitation exhibited more stable and accurate simulations overall, with a higher NSE value (NSE=0.68).

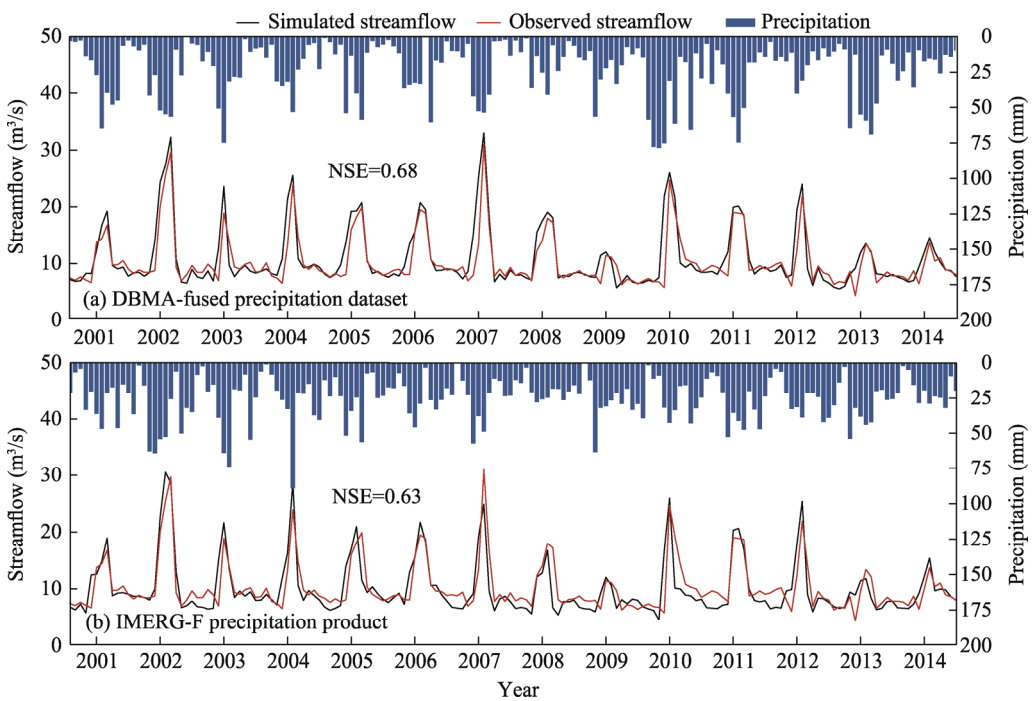

Fig. 9 Comparison of simulated streamflow from the VIC model driven by DBMA-fused precipitation dataset (a) and IMERG-F precipitation product (b) with observed streamflow from the Wenquan hydrological station in the Ebinur Lake Basin from 2001 to 2014. VIC, Variable Infiltration Capacity; IMERG-F, Integrated Multi-satellitE Retrievals for Global Precipitation Measurement Final; NSE, Nash-Sutcliffe efficiency.

5 Discussion

5.1 Rationality analysis

Satellite-based and reanalysis precipitation estimates are particularly important alternative solutions for hydrological applications in ungauged areas and regions with restricted availability of precipitation information (Zambrano et al., 2017). In this paper, six domestic and foreign satellite-based and reanalysis precipitation datasets were selected, and their applicability in Xinjiang, China, was comprehensively evaluated using traditional evaluation methods based on ground-based observational precipitation data. On the basis of these data, the DBMA approach was used as the core to establish the basic framework for the fusion of multi-source precipitation data. Site validation and assessment of hydrological model-simulated streamflow demonstrated that employing the DBMA approach to fuse individual satellite-based precipitation estimates is reliable in the arid regions of Northwest China.

Comprehensive assessment of the six satellite-based and reanalysis precipitation datasets based on the ground-based observational precipitation data revealed that three high-resolution datasets (CMFD, ERA5-Land, and CHIRPS) provide more accurate representations of the spatial distribution of precipitation in Xinjiang (Hu et al., 2021). Unlike the strong spatial dependence of CHIRPS in the upper and lower reaches of the Indus River Basin, India (Shahid et al., 2021), the spatial dependence of CHIRPS data in Xinjiang of China is limited, and the precipitation distribution is consistent with the actual situation. However, ERA5-Land tends to overestimate the actual precipitation on the northern slopes of the Tianshan Mountains and the Ili River Valley. Chen et al. (2021) reported that ERA5-Land precipitation estimates can effectively reflect the obstructive effect of terrain. The Tianshan Mountains and Altay Mountains block moisture from the Atlantic and Arctic Oceans and form precipitation centers on windward mountain slopes, resulting in reduced water vapor transport into the southern region of Xinjiang (Zambrano et al., 2017). The evaluation results showed that CMFD performs best in terms of precipitation detection because of its high correlation with "actual" precipitation at different time scales and low data bias. This difference is attributed mainly to the fact that the production process is augmented with a greater abundance of *in situ* station-based observational data coupled with the integration of surface measurements and remote sensing fusion algorithms, resulting in superior performance over Global Land Data Assimilation System (GLDAS) in western China (He et al., 2020). Additionally, consistent conclusions are reached in the evaluation of precipitation datasets in the Tibetan Plateau region of China, with CMFD product exhibiting greater accuracy at different time scales than TMPA, CHIRPS, and ERA5-Land datasets (Wu et al., 2019; Liu et al., 2023). In contrast, CMORPH performs the poorest across different time scales, which is evident in winter precipitation monitoring, where the occurrence is only 2% and the FAR is as high as 0.90. Relevant research has shown that passive microwave precipitation retrieval techniques cannot easily separate precipitation radiative signals from ice-covered frozen areas (Behrangi et al., 2014), usually assigning zero to missing precipitation data (Mei et al., 2014). Given that a significant portion of Xinjiang is covered by ice or snow in winter, CMORPH precipitation estimates are highly susceptible to ice and snow cover, and the rain gauge correction algorithm does not seem to ameliorate this situation, thus making CMORPH less suitable as an alternative for winter precipitation estimates in ice-covered frozen areas (Zhang et al., 2018). Moreover, CMORPH has more severe precipitation misrepresentation around inland water bodies, warranting cautious use for regions containing large water bodies (Guo et al., 2017).

The DBMA approach calculates optimal relative weights for each ensemble member based on ground-based observational precipitation data; it also creates a predictive PDF for merged precipitation through statistical ensemble blending and returns the predictive distribution of individual variables as a weighted average of the posterior distribution (Raftery et al., 2005). Each member's relative weight score is proportional to its performance during the training time period, indicating the uncertainty of individual predictions more strongly. In this study, CMFD and ERA5-Land datasets significantly outperform the other satellite-based and reanalysis precipitation

datasets and consistently contribute the highest relative weights among the combined members in each season (Fig. 6). The likelihood of individual merged members serving as a scale to measure the consistency between precipitation estimates and observed precipitation enables the combined DBMA data to benefit from well-performing members and obtain higher relative weights (Sloughter et al., 2007), which is verified by the accuracy evaluation results of the above precipitation datasets in Xinjiang. In addition, the streamflow simulation of the combined DBMA-fused precipitation data in the Ebinur Lake Basin captures most of the streamflow peaks and is more robust than the IMERG-F precipitation product. The slightly overestimation of summer streamflow by DBMA-fused precipitation is partly due to the higher relative weights assigned to CMFD and ERA5-Land for fusion precipitation, which generally overestimates actual precipitation throughout the year. The other side lies in the reduction in river streamflow due to unnatural factors (e.g., increased human withdrawals in summer) (Bao et al., 2022). Thus, it is beneficial to find appropriate precipitation data for merging in Xinjiang, where meteorological stations are sparsely distributed and located in regions with complex topography and climate variability; further research or updating of the existing DBMA framework to include new and improved data sources is needed. For example, the use of an HRLT (high-resolution (temporal resolution of 1 d and spatial resolution of 1 km) and long-term (1961–2019)) dataset with higher spatial resolution is recommended in future related studies (Qin et al., 2022).

5.2 Uncertainty analysis

Accurate precipitation estimates are very difficult to obtain in regions with sparse or unmeasured meteorological stations. As an alternative approach, satellite-based or reanalysis precipitation dataset provides homogeneous precipitation estimates at regional or global scales. In this study, by applying DBMA approach, six satellite-based and reanalysis precipitation products at different grid scales were fused with adequate error assessment and successfully applied to the arid region of Northwest China, i.e., Xinjiang, which has complex topography and changeable climate. Nevertheless, the uncertainties inherent in this study still warrant attention.

(1) The limitation of traditional evaluation methods lies in their ability to assess precipitation products only against meteorological stations, with observation errors related to precipitation in regions lacking rain gauges remaining unaddressed, especially in the arid regions of Northwest China with complex topography and variable climate (Zhang et al., 2018; Hasan et al., 2023). In addition, the scale mismatch between gridded estimates and station-based rain gauge measurements may be one of the sources of errors in traditional gridded precipitation product evaluation methods (Ebrahimi et al., 2017).

(2) The weight gridding of DBMA approach considers spatial dependence, and the relative weight scores of unmeasured regions are obtained by interpolating the individual best weights of surrounding stations via the ordinary Kriging interpolation method. Notably, the spatial distribution of meteorological stations in Xinjiang is very uneven and sparse, so there is a large uncertainty in the interpolation process. Additionally, the choice of interpolation algorithm may lead to DBMA-fused precipitation data having different applicability in this region (Hu et al., 2016).

(3) The predicted distribution of cumulative precipitation is asymmetric and consists of two main parts: a large amount of precipitation is zero, and the distribution of the nonzero component follows a gamma distribution (Sloughter et al., 2007). However, the fact that the predicted distributions of individuals follow a Gaussian distribution is a necessary condition for using the DBMA approach. Ma et al. (2018) applied Box–Cox transformation to nonnormal precipitation distribution to estimate normality before applying the DBMA approach, while this study used the "discrete–continuous" model to fit the nonnormal distribution of precipitation. The transformation and fitting of the predicted cumulative precipitation distribution greatly affect the computation of individual weights in DBMA approach. Hence, choosing an appropriate fitting method that aligns with the precipitation characteristics within the study area is of the utmost importance. Box–Cox transformation of precipitation distribution can be used to study the DBMA-fused precipitation in

the future.

(4) The satellite-based and reanalysis precipitation datasets used for DBMA fusion have different spatial resolutions. It is necessary to apply bilinear interpolation to certain precipitation data to standardize them to a spatial resolution of 0.1°. According to the theory of error propagation, the errors generated in the interpolation process further increase the uncertainty in the merging of individual members (Abdollahipour et al., 2021), rising the potential risk to the adaptability of fused precipitation in Xinjiang. Therefore, the fusion process is recommended for selecting multi-source precipitation data with the same spatial resolution to minimize the use of interpolation methods.

6 Conclusions

In the present study, we evaluated the applicability of six satellite-based and reanalysis precipitation products (CHIRPS, CMFD, CMORPH, PERSIANN-CDR, TMPA, and ERA5-Land) in Xinjiang at both temporal and spatial scales. Thus, a general framework for merging precipitation data with different spatial resolutions with DBMA approach as the core was proposed. We calculated the daily optimal DBMA weights of the members during 1999–2018 and utilized the ordinary Kriging interpolation method to spread the station-based relative weights across the entire Xinjiang region; the weighted sum of each precipitation product constitutes the DBMA-fused precipitation. The main findings of the study are summarized as follows:

(1) Among the six satellite-based and reanalysis precipitation products, CMFD exhibits the highest reliability in capturing the spatial pattern of precipitation and performing a statistical analysis of daily precipitation. ERA5-Land performs well in terms of fitting and error analysis of winter precipitation but it tends to overestimate precipitation in terms of precipitation centers. CMORPH is considered unsuitable as an alternative precipitation dataset in Xinjiang, especially for winter precipitation. The accuracy and actual precipitation detection capability of all the satellite-based and reanalysis precipitation products are better in summer.

(2) The average relative weights of CMFD and ERA5-Land datasets are 0.57 and 0.38, respectively. CMORPH has an average relative weight of 0.02, with a peak of 0.08 in late summer and early autumn. The remaining precipitation datasets have the average relative weights of approximately 0.01. Based on the seasonal distribution of average relative weights alone, CMFD has higher relative weights in summer and autumn than in spring and winter, while ERA5-Land shows the opposite pattern.

(3) The performance of DBMA-fused precipitation data evaluated at the independent meteorological stations in Xinjiang is generally satisfactory, showing a CC value of 0.67 with the ground-based observational precipitation. The improvement of DBMA-fused precipitation over the best merged member (CMFD) reaches 7.46% in CC, and its improvement in RMSE reaches 21.35%. Importantly, DBMA-fused precipitation improves the ability of actual precipitation detection events (POD=0.92).

(4) The advancement of DBMA-fused precipitation data is more obvious than that of the most advanced IMERG-F data, with improvements in the performances of different indicators being above 19%. The streamflow simulation results in the Ebinur Lake Basin showed that the use of DBMA-fused precipitation as the hydrological driver of the VIC model is the most effective in streamflow simulation, and its NSE exceeds that of IMERG-F precipitation dataset. The DBMA-fused precipitation can capture most of the streamflow peaks.

Overall, the proposed dynamic-based BMA precipitation fusion process is feasible for the entire Xinjiang region. In the future, it would be beneficial to consider data sources that exhibit better consistency with the study area for the fusion of multiple precipitation sources in this region.

Conflict of interest

DING Jianli is an editorial board member of Journal of Arid Land and was not involved in the editorial review or the decision to publish this article. All authors declare that there are no competing interests.

Acknowledgements

This work was financially supported by The Technology Innovation Team (Tianshan Innovation Team), Innovative Team for Efficient Utilization of Water Resources in Arid Regions (2022TSYCTD0001), the National Natural Science Foundation of China (42171269), and the Xinjiang Academician Workstation Cooperative Research Project (2020.B-001).

Author contributions

Conceptualization: XU Wenjie, DING Jianli; Methodology: XU Wenjie, BAO Qingling; Data curation: XU Wenjie, XU Kun; Writing - review and editing: XU Wenjie; Project administration: DING Jianli, WANG Jinjie; Supervision: DING Jianli; Writing - review and editing: DING Jianli, BAO Qingling; Validation: XU Wenjie, BAO Qingling; Resources: WANG Jinjie; Funding acquisition: DING Jianli, WANG Jinjie. All authors approved the manuscript.

References

Abdollahipour A, Ahmadi H, Aminnejad B. 2021. A review of downscaling methods of satellite-based precipitation estimates. Earth Science Informatics, 15(1): 1–20.

Ashouri H, Hsu K L, Sorooshian S, et al. 2015. PERSIANN-CDR: Daily precipitation climate data record from multisatellite observations for hydrological and climate studies. Bulletin of the American Meteorological Society, 96(1): 69–83.

Baez-Villanueva O M, Zambrano-Bigiarini M, Beck H E, et al. 2020. RF-MEP: A novel Random Forest method for merging gridded precipitation products and ground-based measurements. Remote Sensing of Environment, 239: 111606, doi: 10.1016/j.rse.2019.111606.

Bai X, Wang P, He Y, et al. 2021. Assessing the accuracy and drought utility of long-term satellite-based precipitation estimation products using the triple collocation approach. Journal of Hydrology, 603: 127098, doi: 10.1016/j.jhydrol.2021.127098.

Bao Q, Ding J, Han L, et al. 2022. Quantifying the effects of human activities and climate variability on runoff changes using variable infiltration capacity model. PloS ONE, 17(9): e0272576, doi: 10.1371/journal.pone.0272576.

Behrangi A, Andreadis K, Fisher J B, et al. 2014. Satellite-based precipitation estimation and its application for streamflow prediction over mountainous western U.S. basins. Journal of Applied Meteorology and Climatology, 53(12): 2823–2842.

Chen F, Crow W T, Bindlish R, et al. 2018. Global-scale evaluation of SMAP, SMOS and ASCAT soil moisture products using triple collocation. Remote Sensing of Environment, 214: 1–13.

Chen F C, Jahanshahi M R. 2018. NB-CNN: Deep learning-based crack detection using convolutional neural network and Naïve Bayes data fusion. IEEE Transactions on Industrial Electronics, 65(5): 4392–4400.

Chen Y, Sharma S, Zhou X, et al. 2021. Spatial performance of multiple reanalysis precipitation datasets on the southern slope of Central Himalaya. Atmospheric Research, 250: 105365, doi: 10.1016/j.atmosres.2020.105365.

Dinku T, Funk C, Peterson P, et al. 2018. Validation of the CHIRPS satellite rainfall estimates over eastern Africa. Quarterly Journal of the Royal Meteorological Society, 144(S1): 292–312.

Ebrahimi S, Chen C, Chen Q, et al. 2017. Effects of temporal scales and space mismatches on the TRMM 3B42 v7 precipitation product in a remote mountainous area. Hydrological Processes, 31(24): 4315–4327.

Funk C, Peterson P, Landsfeld M, et al. 2015. The climate hazards infrared precipitation with stations—a new environmental record for monitoring extremes. Scientific Data, 2(1): 1–21.

Gebregiorgis A S, Hossain F. 2015. How well can we estimate error variance of satellite precipitation data around the world? Atmospheric Research, 154: 39–59.

Guo H, Bao A, Ndayisaba F, et al. 2017. Systematical evaluation of satellite precipitation estimates over central Asia using an improved error-component procedure. Journal of Geophysical Research: Atmospheres, 122(20): 10906–10927.

Hasan M A, Mia M B, Khan M R, et al. 2023. Temporal changes in land cover, land surface temperature, soil moisture, and evapotranspiration using remote sensing techniques—a case study of Kutupalong Rohingya Refugee Camp in Bangladesh. Journal of Geovisualization and Spatial Analysis, 7(1): 11, doi: 10.1007/s41651-023-00140-6.

He J, Yang K, Tang W, et al. 2020. The first high-resolution meteorological forcing dataset for land process studies over China. Scientific data, 7(1): 25, doi: 10.1038/s41597-020-0369-y.

Hoeting J A, Madigan D, Raftery A E, et al. 1998. Bayesian model averaging. Proceedings of the AAAI Workshop on Integrating Multiple Learned Models, 335: 77–83.

Hong Y, Hsu K L, Sorooshian S, et al. 2004. Precipitation estimation from remotely sensed imagery using an artificial neural

network cloud classification system. Journal of Applied Meteorology, 43(12): 1834–1853.

Hou A Y, Kakar R K, Neeck S, et al. 2014. The global precipitation measurement mission. Bulletin of the American Meteorological Society, 95(5): 701–722.

Hu W, Yao J, He Q, et al. 2021. Changes in precipitation amounts and extremes across Xinjiang (northwest China) and their connection to climate indices. PeerJ, 9: e10792, doi: 10.7717/peerj.10792.

Hu Z, Hu Q, Zhang C, et al. 2016. Evaluation of reanalysis, spatially interpolated and satellite remotely sensed precipitation data sets in Central Asia. Journal of Geophysical Research: Atmospheres, 121(10): 5648–5663.

Huffman G J, Bolvin D T, Nelkin E J, et al. 2007. The TRMM Multisatellite Precipitation Analysis (TMPA): quasi-global, multiyear, combined-sensor precipitation estimates at fine scales. Journal of Hydrometeorology, 8(1): 38–55.

Jiang S, Ren L, Hong Y, et al. 2012. Comprehensive evaluation of multi-satellite precipitation products with a dense rain gauge network and optimally merging their simulated hydrological flows using the Bayesian model averaging method. Journal of Hydrology, 452–453: 213–225.

Joyce R J, Janowiak J E, Arkin P A, et al. 2004. CMORPH: A method that produces global precipitation estimates from passive microwave and infrared data at high spatial and temporal resolution. Journal of Applied Hydrometeorology, 5(3): 487–503.

Katipoğlu O M. 2022. Spatial analysis of seasonal precipitation using various interpolation methods in the Euphrates Basin, Turkey. Acta Geophysica, 70(2): 859–878.

Kharaghani H, Etemadfard H, Golmohammadi M. 2023. Spatio-temporal analysis of precipitation effects on bicycle-sharing systems with tensor approach. Journal of Geovisualization and Spatial Analysis, 7(2): 30, doi: 10.1007/s41651-023-00161-1.

Lanza L G, Stagi L. 2008. Certified accuracy of rainfall data as a standard requirement in scientific investigations. Advances in Geosciences, 16: 43–48.

Li X, Tsai F T C. 2009. Bayesian model averaging for groundwater head prediction and uncertainty analysis using multimodel and multimethod. Water Resources Research, 45(9): W09403, doi: 10.1029/2008WR007488.

Liu J, Zhou Y, Lu F, et al. 2023. Evaluating satellite- and reanalysis-based precipitation products over the Qinghai-Tibetan Plateau in the perspective of a new error-index system. International Journal of Climatology, 43(5): 2200–2219.

Ma Y, Hong Y, Chen Y, et al. 2018. Performance of optimally merged multisatellite precipitation products using the dynamic Bayesian model averaging scheme over the Tibetan Plateau. Journal of Geophysical Research: Atmospheres, 123(2): 814–834.

Mei Y, Anagnostou E N, Nikolopoulos E I, et al. 2014. Error analysis of satellite precipitation products in mountainous basins. Journal of Hydrometeorology, 15(5): 1778–1793.

Mosaffa H, Shirvani A, Khalili D, et al. 2020. Post and near real-time satellite precipitation products skill over Karkheh River Basin in Iran. International Journal of Remote Sensing, 41(17): 6484–6502.

Muñoz-Sabater J, Dutra E, Agustí-Panareda A, et al. 2021. ERA5-Land: A state-of-the-art global reanalysis dataset for land applications. Earth System Science Data, 13(9): 4349–4383.

Qin R, Zhao Z, Xu J, et al. 2022. HRLT: a high-resolution (1 d, 1 km) and long-term (1961–2019) gridded dataset for surface temperature and precipitation across China. Earth System Science Data, 14(11): 4793–4810.

Raftery A E, Gneiting T, Balabdaoui F, et al. 2005. Using Bayesian model averaging to calibrate forecast ensemble. Monthly Weather Review, 133(5): 1155–1174.

Rings J, Vrugt J A, Schoups G, et al. 2012. Bayesian model averaging using particle filtering and Gaussian mixture modeling: Theory, concepts, and simulation experiments. Water Resources Research, 48(5): W05520, doi: 10.1029/2011WR011607.

Rogelis M C, Werner M. 2018. Streamflow forecasts from WRF precipitation for flood early warning in mountain tropical areas. Hydrology and Earth System Sciences, 22(1): 853–870.

Schöniger A, Wöhling T, Samaniego L, et al. 2014. Model selection on solid ground: Rigorous comparison of nine ways to evaluate Bayesian model evidence. Water Resources Research, 50(12): 9484–9513.

Shahid M, Rahman K U, Haider S, et al. 2021. Assessing the potential and hydrological usefulness of the CHIRPS precipitation dataset over a complex topography in Pakistan. Hydrological Sciences Journal, 66(11): 1664–1684.

Shen Y, Xiong A. 2016. Validation and comparison of a new gauge-based precipitation analysis over mainland China. International Journal of Climatology, 36(1): 252–265.

Sloughter J M L, Raftery A E, Gneiting T, et al. 2007. Probabilistic quantitative precipitation forecasting using Bayesian model averaging. Monthly Weather Review, 135(9): 3209–3220.

Sun S, Wang J, Shi W, et al. 2021. Capacity of the PERSIANN-CDR product in detecting extreme precipitation over Huai River Basin, China. Remote Sensing, 13(9): 1747, doi: 10.3390/rs13091747.

Tadesse K E, Melesse A M, Awas A A, et al. 2022. Evaluation of merging method for CHIRP satellite rainfall estimate over Wabi Shebelle River Basin, Ethiopia. Journal of the Indian Society of Remote Sensing, 50(11): 2125–2138.

Tan M L, Santo H. 2018. Comparison of GPM IMERG, TMPA 3B42 and PERSIANN-CDR satellite precipitation products over Malaysia. Atmospheric Research, 202: 63–76.

Tang G, Long D, Hong Y. 2016. Systematic anomalies over inland water bodies of high mountain Asia in TRMM precipitation estimates: no longer a problem for the GPM era? IEEE Geoscience and Remote Sensing Letters, 13(12): 1762–1766.

Tang G, Clark M P, Papalexiou S M, et al. 2020. Have satellite precipitation products improved over last two decades? A comprehensive comparison of GPM IMERG with nine satellite and reanalysis datasets. Remote Sensing of Environment, 240: 111697, doi: 10.1016/j.rse.2020.111697.

Ur Rahman K, Shang S, Shahid M, et al. 2019. An appraisal of dynamic Bayesian model averaging-based merged multi-Satellite precipitation datasets over complex topography and the diverse climate of Pakistan. Remote Sensing, 12(1): 10, doi: 10.3390/rs12010010.

Wang C, Si J, Zhao C, et al. 2022. Adequacy of satellite derived data for streamflow simulation in three Hexi inland river basins, Northwest China. Atmospheric Research, 274: 106203, doi: 10.1016/j.atmosres.2022.106203.

Wang Q, Xia J, She D, et al. 2021. Assessment of four latest long-term satellite-based precipitation products in capturing the extreme precipitation and streamflow across a humid region of southern China. Atmospheric Research, 257: 105554, doi: 10.1016/j.atmosres.2021.105554.

Wang Z, Zhong R, Lai C, et al. 2017. Evaluation of the GPM IMERG satellite-based precipitation products and the hydrological utility. Atmospheric Research, 196: 151–163.

Wei L, Jiang S, Dong J, et al. 2023a. Fusion of gauge-based, reanalysis, and satellite precipitation products using Bayesian model averaging approach: Determination of the influence of different input sources. Journal of Hydrology, 618: 129234, doi: 10.1016/j.jhydrol.2023.129234.

Wei Y, Law A W K, Yang C. 2023b. Probabilistic optimal interpolation for data assimilation between machine learning model predictions and real time observations. Journal of Computational Science, 67: 101977, doi: 10.1016/j.jocs.2023.101977.

Wu Y, Guo L, Zheng H, et al. 2019. Hydroclimate assessment of gridded precipitation products for the Tibetan Plateau. Science of the Total Environment, 660: 1555–1564.

Xu L, Chen N, Moradkhani H, et al. 2020. Improving global monthly and daily precipitation estimation by fusing gauge observations, remote sensing, and reanalysis data sets. Water Resources Research, 56(3): e2019WR026444, doi: 10.1029/2019wr026444.

Yang T, Li Q, Chen X, et al. 2020. Spatiotemporal variability of the precipitation concentration and diversity in Central Asia. Atmospheric Research, 241: 104954, doi: 10.1016/j.atmosres.2020.104954.

Yin G, Li L, Meng X, et al. 2017. A research of precipitation trend and fluctuation in Xinjiang from 1979 to 2013. Journal of North China University of Water Resources and Electric Power, 38(5): 19–27. (in Chinese)

Yin J, Guo S, Gu L, et al. 2021. Blending multi-satellite, atmospheric reanalysis and gauge precipitation products to facilitate hydrological modelling. Journal of Hydrology, 593: 125878, doi: 10.1016/j.jhydrol.2020.125878.

Yumnam K, Guntu R K, Rathinasamy M, et al. 2022. Quantile-based Bayesian Model Averaging approach towards merging of precipitation products. Journal of Hydrology, 604: 127206, doi: 10.1016/j.jhydrol.2021.127206.

Zambrano F, Wardlow B, Tadesse T, et al. 2017. Evaluating satellite-derived long-term historical precipitation datasets for drought monitoring in Chile. Atmospheric Research, 186: 26–42.

Zhang C, Chen X, Shao H, et al. 2018. Evaluation and intercomparison of high-resolution satellite precipitation estimates—GPM, TRMM, and CMORPH in the Tianshan Mountain Area. Remote Sensing, 10(10): 1543, doi: 10.3390/rs10101543.

Zhang Y, Long A, Lv T, et al. 2022. Trends, cycles, and spatial distribution of the precipitation, potential evapotranspiration and aridity index in Xinjiang, China. Water, 15(1): 62, doi: 10.3390/w15010062.